

Multi-agent-based Rolling Optimization Method for Restoration Scheduling of Distribution Systems with Distributed Generation

Donghan Feng, *Senior Member, IEEE*, Fan Wu, *Student Member, IEEE*, Yun Zhou, *Member, IEEE*, Usama Rahman, Xiaojin Zhao, and Chen Fang

Abstract—Resilience against major disasters is the most essential characteristic of future electrical distribution systems (EDSs). A multi-agent-based rolling optimization method for EDS restoration scheduling is proposed in this paper. When a blackout occurs, considering the risk of losing the centralized authority due to the failure of the common core communication network, the available agents after disasters or cyber-attacks identify the communication-connected parts (CCPs) in the EDS with distributed communication. A multi-time interval optimization model is formulated and solved by the agents for the restoration scheduling of a CCP. A rolling optimization process for the entire EDS restoration is proposed. During the scheduling/rescheduling in the rolling process, CCPs in EDS are re-identified and the restoration schedules for CCPs are updated. Through decentralized decision-making and rolling optimization, EDS restoration scheduling can automatically start and periodically update itself, providing an effective solution for EDS restoration scheduling in a blackout event. A modified IEEE 123-bus EDS is utilized to demonstrate the effectiveness of the proposed method.

Index Terms—Electrical distribution system, restoration scheduling, multi-agent system, rolling optimization.

I. INTRODUCTION

As the utility electrical infrastructure ages and the demand for electricity continues to increase, the impacts of major interruptions of the electrical infrastructure will be more intense [1]. Resilience against major disasters such as

Manuscript received: November 16, 2018; accepted: September 5, 2019. Date of CrossCheck: September 5, 2019. Date of online publication: February 28, 2020.

This work was supported in part by National Key R&D Program of China (No. 2018YFB0905000), in part by the Science and Technology Project of State Grid Corporation of China (No. SGITDK00DWJS1800232), in part by the National Natural Science Foundation of China (No. 51907122), and in part by the Shanghai Sailing Program (No. 19YF1423800).

This article is distributed under the terms of the Creative Commons Attribution 4.0 International License (<http://creativecommons.org/licenses/by/4.0/>).

D. Feng, F. Wu, Y. Zhou (corresponding author), U. Rahman, and X. Zhao are with the Key Laboratory of Control of Power Transmission and Conversion of the Ministry of Education, Department of Electrical Engineering, Shanghai Jiao Tong University, Shanghai, China (e-mail: seed@sjtu.edu.cn; nanflas.will@sjtu.edu.cn; yun.zhou@sjtu.edu.cn; usama.rehan21@sjtu.edu.cn; zhaoxiaojin@sjtu.edu.cn).

C. Fang is with the Electric Power Research Institute, State Grid Shanghai Municipal Electric Power Company, Shanghai, China (email: fangc02@gmail.com).

DOI: 10.35833/MPCE.2018.000801

floods, hurricanes and earthquakes, are considered by the U.S. Department of Energy (DOE) as the most essential characteristic of future electrical distribution systems (EDSs) [2].

In recent worldwide outage events, after a major disaster or cyber-attack, it has taken hours or even days to restore the entire grid, e.g., 6 hours for the Ukraine blackout on December 23, 2015 [3] and 50 hours for the South Australia blackout on September 28, 2016. [4]. In the early restoration stage, if utility power from the transmission grid is unavailable, EDS could consist of a multi-microgrid system made up of several self-healing microgrid islands, each equipped with distributed generators (DGs) and energy storages (ESs) to provide a balancing service to a wider area during the blackouts.

Intelligent algorithms such as genetic algorithms [5] and artificial neural networks [6], have been used in EDS restoration for a long time. Nevertheless, while these methods are proficient in providing an acceptable result under complex restoration requirements, they cannot guarantee the global optimality of the solution theoretically. Fuzzy set-based approaches [7], [8] can provide proper assessments of restoration goals. However, the restoration results are highly dependent on the design of the fuzzy sets, which is based on subjective experience rather than objective estimation. Using a stochastic method to model the uncertainty in an EDS restoration process [9] cannot deal with supplemental resources and the changing topology of EDS. The solution of a stochastic model resorts to a Monte Carlo simulation, which makes this method difficult to be used online.

In this paper, the problem of EDS restoration scheduling problem aims to maximize the total prioritized loads restored in the EDS by forming microgrid islands powered by local distributed generation, including DGs and ESs, in the early restoration stage after a blackout. In [10], DGs, ESs, and electric vehicles (EVs) are considered to provide a continuous and stable power supply to the power loads, and a restoration strategy for the isolated EDS after the blackout is proposed. In [11], taking into account the uncertainty of the load and output of DGs, a robust restoration decision-making model for EDS is established. Considering the microgrid availability, hierarchical restoration schedules can be adopted to restore the critical loads of EDS [12], [13]. The EDS restoration scheduling methods proposed in [10]-[13] are based



on centralized optimization models. However, considering the risk of losing the centralized authority for restoration scheduling in EDS due to physical damage or core communication network failures caused by major disasters or cyber-attacks, decentralized decision-making methods for EDS restoration scheduling should be developed.

A decentralized decision-making environment, e.g., a multi-agent system (MAS), with two-way distributed communication for restoration scheduling can enhance the resilience of EDS in a blackout event. In [14], considering there is only the local communication available, a distributed multi-agent-based method is proposed to achieve an optimal microgrid formation schedule for EDS to restore the critical loads from a power outage. In [10], a distributed multi-agent-based load restoration algorithm for a microgrid is proposed, in which the stability (convergence) of a consensus algorithm is rigorously discussed. An agent-based consensus algorithm is adopted in [14] and [15] for the discovery of global information. Though the time-variant topology of the communication network is considered in both articles, the number of all agents in MAS is fixed and known to each agent. However, this requirement cannot always be satisfied after a disaster when MAS is broken into several connected parts and is inconsistent with the time-variant nature of the restoration process. Therefore, reenergized, repaired and temporarily built agents in the previous restoration duration will join the MAS gradually. The fixed-number agent-based consensus algorithms in [14] and [15] need an alteration to resolve this issue.

EDS restoration scheduling is a multi-time interval optimization problem. The dynamic system state, e.g., newly discovered DGs/ESs, reenergized or repaired agents, repaired buses/feeders, and possible deviations between the actual staged restoration results as well as the optimized schedules will affect the validity of the optimized restoration schedules in the subsequent restoration intervals.

The EDS restoration schedules need periodic revision to tackle these uncertainties. The rolling optimization method is an effective way of dealing with the uncertainty in planning or scheduling. The main idea of ‘rolling’ is rescheduling periodically according to the updated information. In [16] and [17], different rolling-horizon approaches are introduced to deal with the uncertainty associated with renewable energy resources, load consumption or other parameters in an operation optimization.

In this paper, a multi-agent-based rolling optimization method for restoration scheduling of EDS is proposed. A decentralized MAS with two-way distributed communication is proposed for EDS restoration scheduling. In the rolling optimization process, at the first scheduling moment, the communication-connected parts (CCPs) in EDS are first identified by the information discovery process (IDP) of the available agents in EDS at the beginning of the rolling optimization horizon. Secondly, based on the information discovered by IDP, the restoration schedule for each CCP is determined by agents through solving the multi-time interval restoration scheduling optimization model. In the following rescheduling moments, CCPs in EDS are re-identified by all available

agents, and the restoration schedule of EDS is updated.

To the best of our knowledge, this method is the first that applies rolling optimization to EDS restoration scheduling. In the proposed method, through a decentralized online rolling decision-making procedure, EDS restoration scheduling can automatically start and periodically update itself to adjust to the time-varying states and uncertainties of the system. The introduced definite mixed-integer linear programming (MILP) model can provide effective solutions for EDS restoration scheduling in a blackout event.

The rest of this paper is organized as follows. The general multi-time interval optimization model for restoration scheduling is presented in Section II. The multi-agent-based rolling optimization method for EDS restoration scheduling is described in Section III. Case studies to validate the proposed restoration scheduling method are included in Section IV. Eventually, Section V concludes the paper.

II. RESTORATION SCHEDULING OPTIMIZATION MODEL

The general multi-time interval restoration scheduling optimization model for CCP identified in EDS is formulated in this section. The advanced restoration control period, i.e., the rolling optimization horizon, considered for the restoration scheduling optimization model is denoted by T , the discrete time step is denoted by Δt , and the number of time intervals in T is given by $T/\Delta t$.

A. Objective Function

The main objective of the restoration scheduling problem is to maximize the restored load in the given restoration period [11]. The detailed objective function is shown in (1).

$$\max \sum_{n \in N} \sum_{i \in S_{\text{bus}}^{t_c}} (\omega_{L1} P_{L1,i}^{t_c+n\Delta t} + \omega_{L2} P_{L2,i}^{t_c+n\Delta t} + \omega_{L3} P_{L3,i}^{t_c+n\Delta t}) \Delta t \quad (1)$$

where t_c is the beginning moment of the advance restoration control period; $N = \{0, 1, \dots, T/\Delta t - 1\}$ is the set of discrete time intervals in the advance control period; $S_{\text{bus}}^{t_c}$ is the set of buses in the in-use state or that can be restored to the in-use state in $[t_c, t_c + T]$ in the CCP; $P_{L1,i}^{t_c+n\Delta t}$, $P_{L2,i}^{t_c+n\Delta t}$ and $P_{L3,i}^{t_c+n\Delta t}$ are the first-class, second-class and third-class active loads restored at bus i at the discrete time moment $t_c + n\Delta t$, respectively; and ω_{L1} , ω_{L2} and ω_{L3} are the weighting coefficients of the first-class, second-class and third-class loads, respectively.

B. Constraints

The constraints considered in the optimization model are presented in this part, including the network power flow constraints, the radial topology constraints, the bus power generation and load constraints, and other essential constraints.

1) Network Power Flow Constraints

Considering the advanced control period and based on the Distflow method, the network power flow constraints of the radial distribution power network are formulated in (2)-(9).

$$\begin{aligned} \sum_{ki \in S_{\text{feeder}}^{t_c}} P_{ki}^{t_c+n\Delta t} - \sum_{ij \in S_{\text{feeder}}^{t_c}} (P_{ij}^{t_c+n\Delta t} + r_{ij} I_{\text{sqr},ij}^{t_c+n\Delta t}) + \\ P_{G,i}^{t_c+n\Delta t} - P_{L,i}^{t_c+n\Delta t} = 0 \quad i \in S_{\text{bus}}^{t_c}, n \in N_T \end{aligned} \quad (2)$$

$$\sum_{ki \in S_{\text{feeder}}^{t_c}} Q_{ki}^{t_c+n\Delta t} - \sum_{ij \in S_{\text{feeder}}^{t_c}} (Q_{ij}^{t_c+n\Delta t} + x_{ij} I_{\text{sqr},ij}^{t_c+n\Delta t}) + Q_{G,i}^{t_c+n\Delta t} - Q_{L,i}^{t_c+n\Delta t} = 0 \quad i \in S_{\text{bus}}^{t_c}, n \in N_T \quad (3)$$

$$\begin{cases} V_{\text{sqr},i}^{t_c+n\Delta t} - V_{\text{sqr},j}^{t_c+n\Delta t} = 2(P_{ij}^{t_c+n\Delta t} r_{ij} + Q_{ij}^{t_c+n\Delta t} x_{ij}) + (r_y^2 + x_y^2) I_{\text{sqr},ij}^{t_c+n\Delta t} & ij \in S_{\text{feeder}}^{t_c}, n \in N_T \\ w_{ij}^{t_c+n\Delta t} = 1 \end{cases} \quad (4)$$

$$(V_{\text{bus}}^{\text{norm}})^2 I_{\text{sqr},ij}^{t_c+n\Delta t} = f(P_{ij}^{t_c+n\Delta t}, r_{ij} I_{\text{max},ij}^2, \Lambda) + f(Q_{ij}^{t_c+n\Delta t}, x_{ij} I_{\text{max},ij}^2, \Lambda) \quad ij \in S_{\text{feeder}}^{t_c}, n \in N_T \quad (5)$$

$$-w_{ij}^{t_c+n\Delta t} r_{ij} I_{\text{max},ij}^2 \leq P_{ij}^{t_c+n\Delta t} \leq w_{ij}^{t_c+n\Delta t} r_{ij} I_{\text{max},ij}^2 \quad ij \in S_{\text{feeder}}^{t_c}, n \in N_T \quad (6)$$

$$-w_{ij}^{t_c+n\Delta t} x_{ij} I_{\text{max},ij}^2 \leq Q_{ij}^{t_c+n\Delta t} \leq w_{ij}^{t_c+n\Delta t} x_{ij} I_{\text{max},ij}^2 \quad ij \in S_{\text{feeder}}^{t_c}, n \in N_T \quad (7)$$

$$\begin{cases} (V_{\text{bus}}^{\min})^2 \leq V_{\text{sqr},i}^{t_c+n\Delta t} \leq (V_{\text{bus}}^{\max})^2 & i \in S_{\text{bus}}^{t_c}, n \in N_T \\ v_i^{t_c+n\Delta t} = 1 \end{cases} \quad (8)$$

$$\begin{cases} 0 \leq I_{\text{sqr},ij}^{t_c+n\Delta t} \leq I_{\text{max},ij}^2 & ij \in S_{\text{feeder}}^{t_c}, n \in N_T \\ w_{ij}^{t_c+n\Delta t} = 1 \end{cases} \quad (9)$$

Constraints (2) and (3) are the active and reactive power balance equations, where $P_{G,i}^{t_c+n\Delta t}$ and $Q_{G,i}^{t_c+n\Delta t}$ are the active and reactive generation power of bus i at $t_c + n\Delta t$ in $[t_c, t_c + T]$, respectively; $P_{L,i}^{t_c+n\Delta t}$ and $Q_{L,i}^{t_c+n\Delta t}$ are the active and reactive restored loads of bus i , respectively; $S_{\text{feeder}}^{t_c}$ is the set of feeders in the in-use state or that can be restored to the in-use state in $[t_c, t_c + T]$ in the CCP; $P_{ij}^{t_c+n\Delta t}$ and $Q_{ij}^{t_c+n\Delta t}$ are the active and reactive power of feeder ij , respectively; r_{ij} and x_{ij} are the resistance and reactance of feeder ij , respectively; and $I_{\text{sqr},ij}^{t_c+n\Delta t}$ is the quadratic terms of the magnitude of the feeder current.

The voltage difference across feeder ij can be obtained from (4), where $V_{\text{sqr},i}^{t_c+n\Delta t}$ is the quadratic term of the magnitude of the bus voltage. The binary variable $w_{ij}^{t_c+n\Delta t}$ is the state variable of feeder ij , i.e., $w_{ij}^{t_c+n\Delta t} = 1$ for the in-use state and $w_{ij}^{t_c+n\Delta t} = 0$ for the not-in-use state. Note that for the condition constraint in (4) and later in this section, by introducing a sufficiently large constant M , the condition constraint can be transformed into two regular linear constraints.

Constraint (5) is a linear simplification of the equation $V_{\text{sqr},i}^{t_c+n\Delta t} I_{\text{sqr},ij}^{t_c+n\Delta t} = (P_{ij}^{t_c+n\Delta t})^2 + (Q_{ij}^{t_c+n\Delta t})^2$, while the detailed simplification process and definition of the self-optimal piece-wise linear (PWL) approximation function $f(y, \bar{y}, \Lambda)$ can be referred to in [18]. $V_{\text{bus}}^{\text{norm}}$ is the nominal bus voltage magnitude; $I_{\text{max},ij}$ is the upper bound of the current magnitude of feeder ij ; and Λ is the number of discretizations used in the PWL function.

Constraints (6)-(9) are the upper and lower bound limits of $P_{ij}^{t_c+n\Delta t}$, $Q_{ij}^{t_c+n\Delta t}$, $V_{\text{sqr},i}^{t_c+n\Delta t}$ and $I_{\text{sqr},ij}^{t_c+n\Delta t}$, respectively. Similar to $w_{ij}^{t_c+n\Delta t}$, $v_i^{t_c+n\Delta t}$ is the binary state variable of bus i ; and V_{bus}^{\max} and V_{bus}^{\min} are the upper and lower bounds of the bus voltage magnitude, respectively.

In addition, for $v_i^{t_c+n\Delta t}$ and $w_{ij}^{t_c+n\Delta t}$ in (2)-(9) and later in this section, if the in-use state of a bus or feeder is non-optimal for some or all intervals in $[t_c, t_c + T]$, the corresponding $v_i^{t_c+n\Delta t}$ or $w_{ij}^{t_c+n\Delta t}$ should be set to fixed values. Note that the constraints in (2)-(9) are for a balanced EDS and can also be extended for a three-phase unbalanced EDS [19].

2) Radial Topology Constraints

Considering that the number of microgrid islands in the CCP is indeterminate and changeable during different discrete time intervals in the restoration process, e.g., through the merging of existing islands, the radial topology constraints proposed in [11] and [20] may be inapplicable.

$$S_{\text{bus,f}}^{t_c} = S_{\text{bus}}^{t_c} + \{0\} \quad (10)$$

$$S_{\text{feeder,f}}^{t_c} = S_{\text{feeder}}^{t_c} + \{0j \mid j \in S_{\text{bus,DG}}^{t_c} + S_{\text{bus,ES}}^{t_c}\} \quad (11)$$

$$S_{\text{feeder,f,dir}}^{t_c} = \{ij \mid ij \in S_{\text{feeder,f}}^{t_c} \text{ or } ji \in S_{\text{feeder,f}}^{t_c}\} \quad (12)$$

In (11), $S_{\text{bus,DG}}^{t_c}$ and $S_{\text{bus,ES}}^{t_c}$ are the sets of DG and ES buses, respectively, and the name of the fictitious bus (Bus0) is simplified as 0 for simplification in the formulas. Additionally, the sets of buses, feeders, and directed feeders ($S_{\text{bus,f}}^{t_c}$, $S_{\text{feeder,f}}^{t_c}$, $S_{\text{feeder,f,dir}}^{t_c}$) of the directed fictitious network are defined in (10)-(12), respectively.

On the basis of the idea of the fictitious network and fictitious power, directed fictitious network-based radial topology constraints can be suitable for a CCP with an indeterminate number of islands [21]. The schematic diagram of the directed fictitious network of an EDS is shown in Fig. 1. A fictitious bus (Bus0 in Fig. 1) with fictitious feeders connecting the fictitious bus and all DG buses and ES buses is added to the original network and makes up the fictitious network.

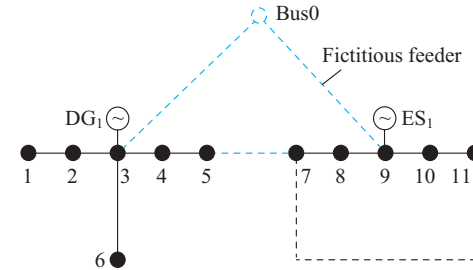


Fig. 1. Directed fictitious network of an EDS with DGs and ESs.

The radial constraints based on the directed fictitious network are presented in (13)-(20).

$$\sum_{ki \in S_{\text{feeder,f,dir}}^{t_c}} H_{ki}^{t_c+n\Delta t} - \sum_{ij \in S_{\text{feeder,f,dir}}^{t_c}} H_{ij}^{t_c+n\Delta t} = v_{f,i}^{t_c+n\Delta t} \quad i \in S_{\text{bus,f}}^{t_c} - \{0\}, n \in N_T \quad (13)$$

$$0 \leq H_{ij}^{t_c+n\Delta t} \leq w_{f,dir,ij}^{t_c+n\Delta t} \mid S_{\text{bus,f}}^{t_c} \quad ij \in S_{\text{feeder,f}}^{t_c}, n \in N_T \quad (14)$$

$$v_{f,i}^{t_c+n\Delta t} + v_{f,j}^{t_c+n\Delta t} \geq 2(w_{f,dir,ij}^{t_c+n\Delta t} + w_{f,dir,ji}^{t_c+n\Delta t}) \quad ij \in S_{\text{feeder,f}}^{t_c}, n \in N_T \quad (15)$$

$$v_{f,i}^{t_c+n\Delta t} = v_i^{t_c+n\Delta t} \quad i \in S_{\text{bus}}^{t_c}, n \in N_T \quad (16)$$

$$w_{f,dir,ij}^{t_c+n\Delta t} + w_{f,dir,ji}^{t_c+n\Delta t} = w_{ij}^{t_c+n\Delta t} \quad ij \in S_{\text{feeder}}^{t_c}, n \in N_T \quad (17)$$

$$v_{f,0}^{t_c+n\Delta t} = 1 \quad n \in N_T \quad (18)$$

$$w_{f,\text{dir},j0}^{t_c+n\Delta t} = 0 \quad j0 \in S_{\text{feeder,f,dir}}^{t_c}, n \in N_T \quad (19)$$

$$\sum_{ki \in S_{\text{feeder,f,dir}}^{t_c}} w_{f,\text{dir},ki}^{t_c+n\Delta t} = v_{f,i}^{t_c+n\Delta t} \quad i \in S_{\text{bus,f}}^{t_c} - \{0\}, n \in N_T \quad (20)$$

In (13), $v_{f,i}^{t_c+n\Delta t}$ is the binary state variable of bus i in the fictitious network and $H_{ij}^{t_c+n\Delta t}$ is the fictitious power of directed feeder ij in the fictitious network. In (14), $w_{f,\text{dir},ij}^{t_c+n\Delta t}$ is the binary state variable of feeder ij in the fictitious network. From (13) and (14), every bus (except Bus0) in the in-use state in the fictitious network has a unit of fictitious load. All fictitious power transmitted in the fictitious network is generated from Bus0. The fictitious power balance equation in (13) ensures the connection of the fictitious network (all buses and feeders in the in-use state).

The constraints of the state variables of buses and feeders in the directed fictitious network are described in (15)-(19). The relationship between the bus and feeder state variables is indicated in (15). The mapping relationships of the state variables in the fictitious network and the original network are represented in (16) and (17), respectively. The default values of Bus0 and fictitious feeders pointed to Bus0 are set in (18) and (19), respectively.

For a connected network including all buses and feeders in the in-use state, constraint (20) makes every bus (except Bus0) in the in-use state have only one parent bus, which ensures that the connected network is a tree-like branching network. From constraints (13)-(20), the radial topology of the fictitious network can be guaranteed, and accordingly, the radial topology of all microgrid islands in CCP (the original network) can be guaranteed.

3) Bus Power Generation and Load Constraints

The bus power generation and load constraints in the multi-time interval optimization model are formulated in (21)-(45) in this part.

$$P_{G,i}^{t_c+n\Delta t} = 0 \quad i \in S_{\text{bus}}^{t_c} - S_{\text{bus,DG}}^{t_c} - S_{\text{bus,ES}}^{t_c}, n \in N_T \quad (21)$$

$$Q_{G,i}^{t_c+n\Delta t} = 0 \quad i \in S_{\text{bus}}^{t_c} - S_{\text{bus,DG}}^{t_c} - S_{\text{bus,ES}}^{t_c}, n \in N_T \quad (22)$$

In (21) and (22), $P_{G,i}^{t_c+n\Delta t}$ and $Q_{G,i}^{t_c+n\Delta t}$ are limited to zero for buses without DG or ES, respectively.

$$P_{G,i}^{t_c+n\Delta t} = P_{DG,i}^{t_c+n\Delta t} \quad i \in S_{\text{bus,DG}}^{t_c}, n \in N_T \quad (23)$$

$$Q_{G,i}^{t_c+n\Delta t} = Q_{DG,i}^{t_c+n\Delta t} \quad i \in S_{\text{bus,DG}}^{t_c}, n \in N_T \quad (24)$$

$$v_i^{t_c+n\Delta t} P_{DG,i}^{\min} \leq P_{DG,i}^{t_c+n\Delta t} \leq v_i^{t_c+n\Delta t} P_{DG,i}^{\max} \quad i \in S_{\text{bus,DG}}^{t_c}, n \in N_T \quad (25)$$

$$\begin{cases} P_{DG,i}^{t_c+n\Delta t} = 0 \\ t_c + n\Delta t < t_{DG,\text{start},i}^{t_c} + T_{DG,i}^{\text{syn}} \end{cases} \quad i \in S_{\text{bus,DG}}^{t_c}, n \in N_T \quad (26)$$

$$\begin{cases} -v_i^{t_c+n\Delta t} P_{DG,\text{ramp},i}^{\max} \leq P_{DG,i}^{t_c+(n+1)\Delta t} - \\ \quad P_{DG,i}^{t_c+n\Delta t} \leq v_i^{t_c+n\Delta t} P_{DG,\text{ramp},i}^{\max} \\ t_c + n\Delta t \geq t_{DG,\text{start},i}^{t_c} + T_{DG,i}^{\text{syn}} \end{cases} \quad i \in S_{\text{bus,DG}}^{t_c}, n \in N'_T \quad (27)$$

$$v_i^{t_c+n\Delta t} \frac{P_{DG,i}^{t_c+n\Delta t}}{P_{DG,i}^{\max}} Q_{DG,i}^{\min} \leq Q_{DG,i}^{t_c+n\Delta t} \leq v_i^{t_c+n\Delta t} \frac{P_{DG,i}^{t_c+n\Delta t}}{P_{DG,i}^{\max}} Q_{DG,i}^{\max} \quad i \in S_{\text{bus,DG}}^{t_c}, n \in N_T \quad (28)$$

The power generation constraints for DG buses are presented in (23)-(28). In (23) and (24), $P_{DG,i}^{t_c+n\Delta t}$ and $Q_{DG,i}^{t_c+n\Delta t}$ are the net active and reactive output power of DG at bus i , respectively. In (25), $P_{DG,i}^{\max}$ and $P_{DG,i}^{\min}$ are the upper and lower bounds of $P_{DG,i}^{t_c+n\Delta t}$, respectively. The starting and ramping constraints are depicted in (26) and (27). Referring to a typical DG operation curve in [22], $t_{DG,\text{start},i}^{t_c}$ is the moment when the DG is ready to start up, and $T_{DG,i}^{\text{syn}}$ is the synchronization time parameter of the DG in (26). In (27), $N'_T = \{0, 1, \dots, T/\Delta t - 2\}$ and $P_{DG,\text{ramp},i}^{\max}$ is the upper ramping active power limit parameter of the DG between two adjacent discrete time intervals. In (28), $Q_{DG,i}^{\max}$ and $Q_{DG,i}^{\min}$ are the upper and lower bounds of $Q_{DG,i}^{t_c+n\Delta t}$ when $P_{DG,i}^{t_c+n\Delta t} = P_{DG,i}^{\max}$, respectively.

$$P_{G,i}^{t_c+n\Delta t} = P_{ES,i}^{t_c+n\Delta t} \quad i \in S_{\text{bus,ES}}^{t_c}, n \in N_T \quad (29)$$

$$Q_{G,i}^{t_c+n\Delta t} = Q_{ES,i}^{t_c+n\Delta t} \quad i \in S_{\text{bus,ES}}^{t_c}, n \in N_T \quad (30)$$

$$P_{ES,i}^{t_c+n\Delta t} = P_{ES,\text{ch},i}^{t_c+n\Delta t} - P_{ES,\text{dis},i}^{t_c+n\Delta t} \quad i \in S_{\text{bus,ES}}^{t_c}, n \in N_T \quad (31)$$

$$0 \leq P_{ES,\text{ch},i}^{t_c+n\Delta t} \leq v_{ch,i}^{t_c+n\Delta t} P_{ES,\text{ch},i}^{\max} \quad i \in S_{\text{bus,ES}}^{t_c}, n \in N_T \quad (32)$$

$$0 \leq P_{ES,\text{dis},i}^{t_c+n\Delta t} \leq v_{dis,i}^{t_c+n\Delta t} P_{ES,\text{dis},i}^{\max} \quad i \in S_{\text{bus,ES}}^{t_c}, n \in N_T \quad (33)$$

$$v_{ch,i}^{t_c+n\Delta t} + v_{dis,i}^{t_c+n\Delta t} \leq v_i^{t_c+n\Delta t} \quad i \in S_{\text{bus,ES}}^{t_c}, n \in N_T \quad (34)$$

$$Q_{ES,\text{min},i}^{t_c+n\Delta t} \leq Q_{ES,i}^{t_c+n\Delta t} \leq Q_{ES,\text{max},i}^{t_c+n\Delta t} \quad i \in S_{\text{bus,ES}}^{t_c}, n \in N_T \quad (35)$$

$$SOC_{ES,i}^{t_c+(n+1)\Delta t} - SOC_{ES,i}^{t_c+n\Delta t} = \frac{(P_{ES,\text{ch},i}^{t_c+n\Delta t} \eta_{ch,i} - P_{ES,\text{dis},i}^{t_c+n\Delta t} \eta_{dis,i})\Delta t}{C_{ES,i}} \quad i \in S_{\text{bus,ES}}^{t_c}, n \in N'_T \quad (36)$$

$$SOC_{ES,\text{min},i} \leq SOC_{ES,i}^{t_c+n\Delta t} \leq SOC_{ES,\text{max},i} \quad i \in S_{\text{bus,ES}}^{t_c}, n \in N_T \quad (37)$$

Considering the battery energy storage systems used, the generation power constraints for ES buses are presented in (29)-(37). In (29) and (30), $P_{ES,i}^{t_c+n\Delta t}$ and $Q_{ES,i}^{t_c+n\Delta t}$ are the net active and reactive output power of ES at bus i , respectively. In (31), $P_{ES,\text{ch},i}^{t_c+n\Delta t}$ and $P_{ES,\text{dis},i}^{t_c+n\Delta t}$ are the active charging and discharging power of ES, respectively. In (32) and (33), $P_{ES,\text{ch},i}^{\max}$ and $P_{ES,\text{dis},i}^{\max}$ are the upper bounds of charging and discharging power, respectively; and $v_{ch,i}^{t_c+n\Delta t}$ and $v_{dis,i}^{t_c+n\Delta t}$ are the binary charging and discharging state variables, respectively. Constraint (34) will avoid the ES being operated in charging and discharging modes simultaneously. In (35), $Q_{ES,\text{max},i}^{t_c+n\Delta t}$ and $Q_{ES,\text{min},i}^{t_c+n\Delta t}$ are the upper and lower bounds of $Q_{ES,i}^{t_c+n\Delta t}$, respectively. According to Fig. 2 [23], the set values of $Q_{ES,\text{max},i}^{t_c+n\Delta t}$ and $Q_{ES,\text{min},i}^{t_c+n\Delta t}$ can be simplified as shown in Table I. Constraint (36) represents the state of charge (SOC) variation of an ES, where $SOC_{ES,i}^{t_c+n\Delta t}$ is the SOC of the ES with the upper and lower bounds $SOC_{ES,\text{max},i}$ and $SOC_{ES,\text{min},i}$ in (37); $C_{ES,i}$ is the rated energy capacity of the ES; and $\eta_{ch,i}$ and $\eta_{dis,i}$ are the parameters of charging and discharging efficiency, respectively.

$$P_{L,i}^{t_c+n\Delta t} = P_{L1,i}^{t_c+n\Delta t} + P_{L2,i}^{t_c+n\Delta t} + P_{L3,i}^{t_c+n\Delta t} \quad i \in S_{\text{bus}}^{t_c}, n \in N_T \quad (38)$$

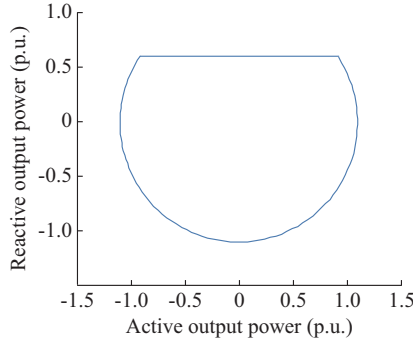


Fig. 2. Reactive power capacity of battery ES system.

TABLE I
ADJUSTABLE RANGE OF ES REACTIVE POWER

Range of $ P_{\text{ES},i}^{t_c+n\Delta t} $ (p.u.)	$[Q_{\text{ES,min},i}^{t_c+n\Delta t}, Q_{\text{ES,max},i}^{t_c+n\Delta t}]$ (p.u.)
[0, 0.2]	[-1.10, 0.60]
(0.2, 0.4]	[-1.00, 0.60]
(0.4, 0.6]	[-0.90, 0.60]
(0.6, 0.8]	[-0.75, 0.60]
(0.8, 1.0]	[-0.50, 0.50]

$$0 \leq P_{\text{L1},i}^{t_c+n\Delta t} \leq v_i^{t_c+n\Delta t} P_{\text{L1,par},i}^{t_c+n\Delta t} \quad i \in S_{\text{bus}}^{t_c}, n \in N_T \quad (39)$$

$$0 \leq P_{\text{L2},i}^{t_c+n\Delta t} \leq v_i^{t_c+n\Delta t} P_{\text{L2,par},i}^{t_c+n\Delta t} \quad i \in S_{\text{bus}}^{t_c}, n \in N_T \quad (40)$$

$$0 \leq P_{\text{L3},i}^{t_c+n\Delta t} \leq v_i^{t_c+n\Delta t} P_{\text{L3,par},i}^{t_c+n\Delta t} \quad i \in S_{\text{bus}}^{t_c}, n \in N_T \quad (41)$$

$$Q_{\text{L1},i}^{t_c+n\Delta t} = Q_{\text{L1},i}^{t_c+n\Delta t} + Q_{\text{L2},i}^{t_c+n\Delta t} + Q_{\text{L3},i}^{t_c+n\Delta t} \quad i \in S_{\text{bus}}^{t_c}, n \in N_T \quad (42)$$

$$Q_{\text{L1},i}^{t_c+n\Delta t} = \frac{P_{\text{L1},i}^{t_c+n\Delta t}}{P_{\text{L1,par},i}^{t_c+n\Delta t}} Q_{\text{L1,par},i}^{t_c+n\Delta t} \quad i \in S_{\text{bus}}^{t_c}, n \in N_T \quad (43)$$

$$Q_{\text{L2},i}^{t_c+n\Delta t} = \frac{P_{\text{L2},i}^{t_c+n\Delta t}}{P_{\text{L2,par},i}^{t_c+n\Delta t}} Q_{\text{L2,par},i}^{t_c+n\Delta t} \quad i \in S_{\text{bus}}^{t_c}, n \in N_T \quad (44)$$

$$Q_{\text{L3},i}^{t_c+n\Delta t} = \frac{P_{\text{L3},i}^{t_c+n\Delta t}}{P_{\text{L3,par},i}^{t_c+n\Delta t}} Q_{\text{L3,par},i}^{t_c+n\Delta t} \quad i \in S_{\text{bus}}^{t_c}, n \in N_T \quad (45)$$

The load constraints in the optimization model are presented in (38)-(45). In (39)-(41), $P_{\text{L1,par},i}^{t_c+n\Delta t}$, $P_{\text{L2,par},i}^{t_c+n\Delta t}$ and $P_{\text{L3,par},i}^{t_c+n\Delta t}$ are the first-class, second-class and third-class active bus load parameters, respectively. In (42), $Q_{\text{L1},i}^{t_c+n\Delta t}$, $Q_{\text{L2},i}^{t_c+n\Delta t}$ and $Q_{\text{L3},i}^{t_c+n\Delta t}$ are the first-class, second-class and third-class reactive loads restored at bus i , respectively. Constraints (43)-(45) ensure that active and reactive loads are restored in proportion, where $Q_{\text{L1,par},i}^{t_c+n\Delta t}$, $Q_{\text{L2,par},i}^{t_c+n\Delta t}$ and $Q_{\text{L3,par},i}^{t_c+n\Delta t}$ are the first-class, second-class and third-class reactive bus load parameters, respectively.

4) Other Essential Constraints

Other essential constraints in the optimization model are formulated in (46)-(52).

$$P_{\text{L},i}^{t_c+n\Delta t} \geq v_i^{t_c+n\Delta t} \lambda_{\min,i} (P_{\text{L1},i}^{t_c+n\Delta t} + P_{\text{L2},i}^{t_c+n\Delta t} + P_{\text{L3},i}^{t_c+n\Delta t}) \quad i \in S_{\text{bus}}^{t_c}, n \in N_T \quad (46)$$

$$P_{\text{L1},i}^{t_c+n\Delta t} \leq P_{\text{L1},i}^{t_c+(n+1)\Delta t} \quad i \in S_{\text{bus}}^{t_c}, n \in N'_T \quad (47)$$

$$P_{\text{L2},i}^{t_c+n\Delta t} \leq P_{\text{L2},i}^{t_c+(n+1)\Delta t} \quad i \in S_{\text{bus}}^{t_c}, n \in N'_T \quad (48)$$

$$v_i^{t_c+n\Delta t} \leq v_i^{t_c+(n+1)\Delta t} \quad i \in S_{\text{bus}}^{t_c}, n \in N'_T \quad (49)$$

$$w_{ij}^{t_c+n\Delta t} \leq w_{ij}^{t_c+(n+1)\Delta t} \quad ij \in S_{\text{feeder}}^{t_c}, n \in N'_T \quad (50)$$

$$\{v_i^{t_c}, w_{ij}^{t_c}\} = \{v_i^{t_c}, w_{ij}^{t_c}\}_{\text{observed}} \quad i \in S_{\text{bus}}^{t_c}, ij \in S_{\text{feeder}}^{t_c} \quad (51)$$

$$\begin{aligned} \{P_{\text{G},i}^{t_c}, P_{\text{L1},i}^{t_c}, P_{\text{L2},i}^{t_c}, P_{\text{L3},i}^{t_c}, \text{SOC}_{\text{ES},i}^{t_c}\} = \\ \{P_{\text{G},i}^{t_c}, P_{\text{L1},i}^{t_c}, P_{\text{L2},i}^{t_c}, P_{\text{L3},i}^{t_c}, \text{SOC}_{\text{ES},i}^{t_c}\}_{\text{observed}} \quad i \in S_{\text{bus}}^{t_c} \end{aligned} \quad (52)$$

Constraint (46) illustrates that if a bus is restored, to ensure the basic function of the bus, a minimum percentage $\lambda_{\min,i}$ of the bus load needs to be restored. The restoration continuity constraints are presented in (47)-(50). The first-class and second-class loads restored in the current discrete time intervals cannot be decreased in later intervals. Additionally, the buses and feeders in the in-use state in the current discrete time interval should maintain the state in later time intervals. In (51) and (52), the boundary conditions of the multi-time interval optimization model, $v_i^{t_c}$, $w_{ij}^{t_c}$, $P_{\text{G},i}^{t_c}$, $P_{\text{L1},i}^{t_c}$, $P_{\text{L2},i}^{t_c}$, $P_{\text{L3},i}^{t_c}$, $\text{SOC}_{\text{ES},i}^{t_c}$, etc., in the first time interval should be set as observed values at the current control moment of the advanced restoration control period.

To summarize, the multi-time interval optimization model of the restoration scheduling problem of CCP is formulated with the objective function in (1) and constraints in (2)-(9) and (13)-(52). As all the constraints are linear constraints with binary variables, the integrated multi-time interval optimization model is an MILP model and can be solved by commercial solvers effectively.

III. MULTI-AGENT-BASED ROLLING OPTIMIZATION PROCESS FOR EDS RESTORATION SCHEDULING

A. Framework of MAS

In this paper, an agent in MAS refers to an individual device or a group of devices which has the ability to acquire local information, control local devices, communicate with other agents, and retain or manipulate the data of the whole distribution system [14]. With a local emergency power source and two-way distributed communication, e.g., through an adhoc network [24], agents can continue to work after a disaster or cyber-attack. After a serious event, the surviving agents can participate in the restoration, while those that are unavailable can be reenergized or repaired and can join the restoration gradually.

The topology of the communication network may differ from that of the distribution system. From the sight of graph theory, an MAS can be regarded as a graph, an available agent can be considered as a node, and a two-way communication link can be considered as an edge. CCP is a maximally connected subgraph of MAS. An example of an MAS with seven agents is shown in Fig. 3. Agent 1 has the computation ability for restoration scheduling. Agent 7 is supposed to be unavailable, while the other agents are available. Accordingly, there exist two CCPs in Fig. 3, and Agents 1-4 form a CCP, while Agents 5 and 6 form another.

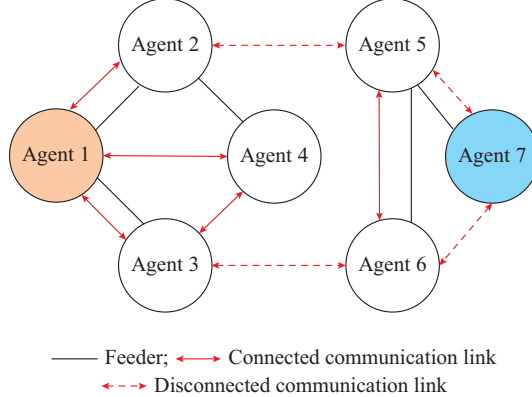


Fig. 3. MAS with seven agents.

B. IDP

In the following part, each bus is supposed to assign an agent. Each agent has the ability to control local devices and save the information of the whole distribution system. Only the information of the load, DGs, ESs, and states of the buses/feeders linked to this bus can be obtained directly. The other information needed for restoration scheduling can be acquired by communicating with the agents nearby. As the distributed generations are the cores of the microgrid islands, the buses with DGs and ESs are assigned agents with the computation ability for restoration scheduling.

Referring to the multi-time interval optimization model formulated in Section II, the information stored in an agent at time t_c must contain the following state information in a CCP.

- 1) Available states of buses: $A_{\text{bus}}^{t_c}$.
- 2) Available states of feeders: $A_{\text{feeder}}^{t_c}$.
- 3) Parameters of feeders: $\{r_{ij}, x_{ij}\}$.
- 4) Energized states of buses: $\{v_i^{t_c}\}$.
- 5) Energized states of feeders: $\{w_{ij}^{t_c}\}$.
- 6) Load restored states of buses: $\{P_{\text{L1},i}^{t_c}, P_{\text{L2},i}^{t_c}, P_{\text{L3},i}^{t_c}\}$ and $\{Q_{\text{L1},i}^{t_c}, Q_{\text{L2},i}^{t_c}, Q_{\text{L3},i}^{t_c}\}$.
- 7) State of DGs: $\{P_{\text{DG},i}^{t_c}\}$ and $\{t_{\text{DG, start},i}^{t_c}\}$.
- 8) State of ESs: $\{SOC_{\text{ES},i}^{t_c}\}$.

If a bus or a feeder is available, its corresponding state is set as 1, and if it is not available, the state is set as 0. These two pieces of information are used to identify the network topology.

The other state information needed for restoration scheduling can be calculated during the scheduling process or pre-stored in the agent. All control variables are derived from the multi-time interval optimization. The agents that finish scheduling can broadcast the values of control variables to other agents in the same CCP.

Under normal conditions, an MAS has a common communication network, and the agents can communicate with each other with no limitations if all requirements for communication are satisfied. After a serious disaster, the common communication network could be destroyed, and the consistent power supply for an agent could be cut off simultaneously. Thus, the communication of an agent would be supported by

limited local power resources so that the communication ability of an agent would be limited. Considering the difficulty in rebuilding common communication and the limited communication ability of agents, a distributed method of communication has to be adopted for IDP in this circumstance. The consensus algorithm is used in IDP. The consensus of agents means that all agents in a CCP of MAS reach an agreement on certain information of this CCP. With limited communication ability, each agent can still obtain the global information of this CCP through an appropriate consensus algorithm. Considering the latency of communication and the time consumption of the data manipulation process, a discrete-form consensus algorithm is preferred. In addition, since a disaster might change the configuration of MAS, the consensus algorithm must be free of information on the topology of the whole system. The average consensus algorithm introduced in [25] is used.

$$X_i^{k+1} = X_i^k + \sum_{j \in N(i)} a_{ij} (X_j^k - X_i^k) \quad k = 0, 1, \dots, k_{\max} \quad (53)$$

where X_i^k is the abstract set of the system parameters known to agent i in the k^{th} iteration; X_i^0 is the information originally owned by agent i , and all parameters referring to the information acquired by other agents are all initiated to 0; k_{\max} is the pre-determined maximum iteration number; $N(i)$ is the set of agents that have the communication with agent i , i.e., neighbors of agent i ; and a_{ij} is the Metropolis-Hastings weight calculated in (54).

$$a_{ij} = \begin{cases} 1/(\max\{n_i, n_j\} + 1) & j \in N(i) \\ 1 - \sum_{k \in N(i)} 1/(\max\{n_i, n_k\} + 1) & j = i \\ 0 & j \notin N(i) \end{cases} \quad (54)$$

where n_i is the number of neighbors of agent i .

The asymptotic result of (53) with the coefficients decided by (54) is:

$$\lim_{k \rightarrow \infty} X_i^k = \frac{1}{N_{\text{a,C}}} \sum_{j=1}^{N_{\text{a,C}}} X_j^0 \quad (55)$$

where $N_{\text{a,C}}$ is the total number of agents in CCP. The convergence of the above consensus algorithm can be proved referring to [15]. It should be emphasized that the validity of applying (53) to MAS depends on the assumption that every communication link in MAS is two-way. Though the choice of a_{ij} may influence the speed of convergence, the design of a_{ij} is beyond the scope of this paper.

In some cases, MAS may be divided into several CCPs after a disaster. Moreover, the recovery of communication is a dynamic process, which makes the topology of each CCP time-variant. Without the knowledge of $N_{\text{a,C}}$ in a CCP, the result of the average consensus algorithm in (55) would be meaningless since only an average result is obtained. To handle this problem, an indicator set with a dynamic size is assigned to every available agent. For agent i , the indicator set I_i is initiated as $I_i^0 = \{(i, 1)\}$, where 1 is the initial indicator corresponding to agent i . Before implementing the consensus algorithm on other values, (53) is applied to the indicator set. Supposing that in the iteration $k+1$, agent i receives the

information of agent j , which may not be directly from agent j , for the first time. Then, I_i^k will be initiated as $I_i^k = I_i^k \cup \{(j, 0)\}$ before (53) is implemented. The indicator corresponding to agent i will achieve $1/N_{a,c}$ asymptotically for all agents in CCP. Then, the value of all parameters needed for scheduling the restoration will be initiated as $N_{a,c}X_i^0$.

By implementing the average consensus algorithm, the information known to any agent will asymptotically approach to the average among each agent in a CCP, which means that all information of this CCP is known to all the agents inside it. A certain CCP has no information about other CCPs. After the synchronous IDP is completed, the restoration scheduling for CCPs will be activated inside each CCP independently.

C. Rolling Optimization Process of EDS Restoration Scheduling

In general, the rolling optimization method transforms a stochastic process into a series of deterministic scenarios. Each scenario lasts a period of time called a horizon. The horizon can be classified into two types: the prediction horizon and the control horizon. A control schedule for the whole prediction horizon is made based on the current information at the beginning of the prediction horizon and will be implemented at the beginning of the control horizon. The prediction horizon and the corresponding control horizon have the same starting time. The control horizon is always shorter than the prediction horizon. The end of a control horizon is the beginning of the next prediction horizon.

Different rolling strategies are utilized in [16] and [17]. In [16], the lengths of the prediction horizon and control horizon are fixed, and both horizons move forward simultaneously. In [17], from the start to the end of a whole scheduling period, the control horizon is fixed, while the prediction horizon decreases gradually from the length of the whole scheduling period to the length of a control horizon. Since the finishing time of the restoration process can hardly be determined, a rolling strategy similar to that in [16] is adopted in this paper.

A number of basic assumptions are made to support the rolling optimization process of EDS restoration scheduling.

1) For each communication link in the MAS, the communication between the two agents is two-way, which ensures that the applied consensus algorithm is always convergent.

2) Each available agent has universal time information, e.g., from GPS timing system. All the agents in the whole distribution system are synchronized at the moment they begin to participate in IDP. IDP and restoration process are triggered by a universal clock.

3) IDP of each agent starts at the same time and is completed before scheduling the restoration. If an agent resumes the communication with other agents during or after an IDP, it cannot join this IDP and has to wait until the next IDP begins. In this circumstance, if the agent is associated with a resource, though the communication with other agents is unavailable, DG can independently start to synchronize at once.

4) Once an agent participates in IDP, it will not discon-

nnect during this IDP.

5) The restoration schedules made for different agents in the same CCP are identical. The agent that firstly finishes the scheduling calculation will broadcast the result to all other agents in CCP.

Controlled by a universal clock, Fig. 4 shows the timeline of the rolling optimized process of EDS restoration scheduling, where t_0 is the restoration starting moment of EDS; T is the rolling optimization horizon, i.e., the prediction horizon; T_r is the rescheduling time gap between two adjacent optimization horizons; and Δt is the discrete time step in the restoration scheduling optimization model for CCPs.

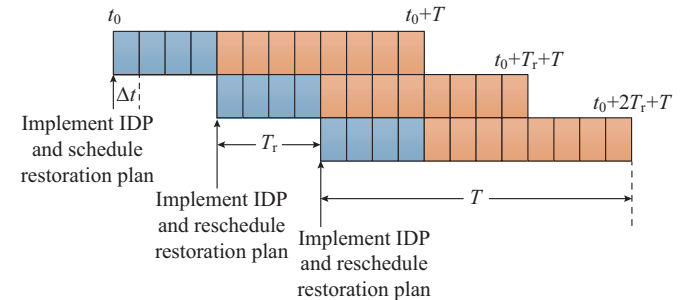


Fig. 4. Timeline of rolling optimized process of EDS restoration scheduling.

The behavior of the agent on a bus with restoration scheduling ability is shown in Fig. 5. The agent firstly implements IDP described in Section III-B and then models the optimization problem described in Section II based on the discovered information. The scheduling and rescheduling results will be broadcasted to all agents in CCP. The other agents have similar behaviors to that shown in Fig. 5, excluding the CCP restoration scheduling step.

IV. CASE STUDY

The proposed multi-agent-based rolling optimization method for restoration scheduling of EDS is tested using a modified IEEE 123-bus EDS. The network topology of the test system is shown in Fig. 6, while the original parameters of this system are obtained from [26]. The weights of the first-class, second-class and third-class of active loads in the test system (ω_{L1} , ω_{L2} , and ω_{L3}) are set as 1000, 100, and 10, respectively. The communication network is supposed to have the same topology as the distribution network, and each bus agent can only communicate with the bus agent adjacent to it. In the rolling optimization process of EDS restoration scheduling shown in Fig. 4, the rolling optimization horizon T is set to 120 min, and the rescheduling time gap T_r is set to 30 min. The discrete time step Δt in the restoration scheduling optimization model for CCP is set to 5 min. For the IDP, the convergence condition of the consensus algorithm is set as the difference between two iterations, at less than 10^{-10} . The proposed multi-agent-based rolling optimization process for EDS restoration scheduling is implemented in MATLAB with YALMIP, and Gurobi is used as the MILP solver.

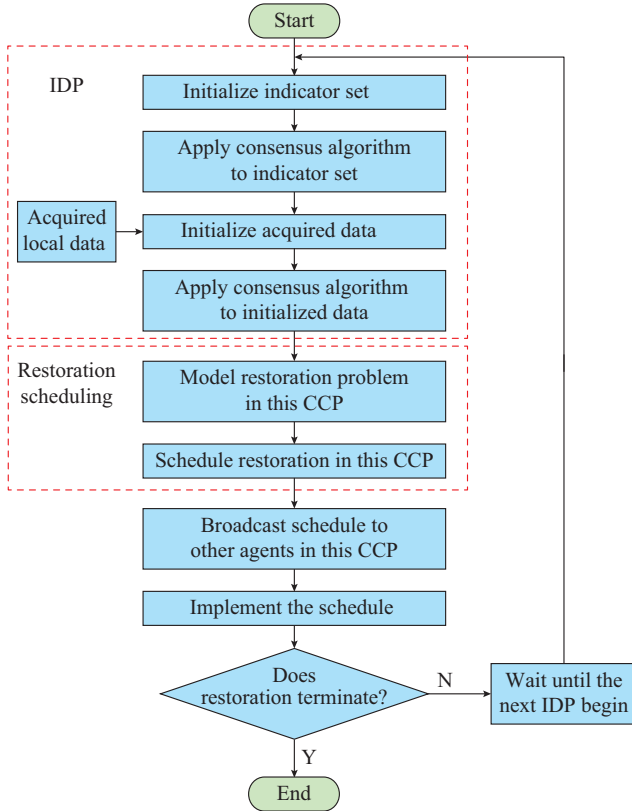


Fig. 5. Behaviors of agent with computation ability for restoration scheduling.

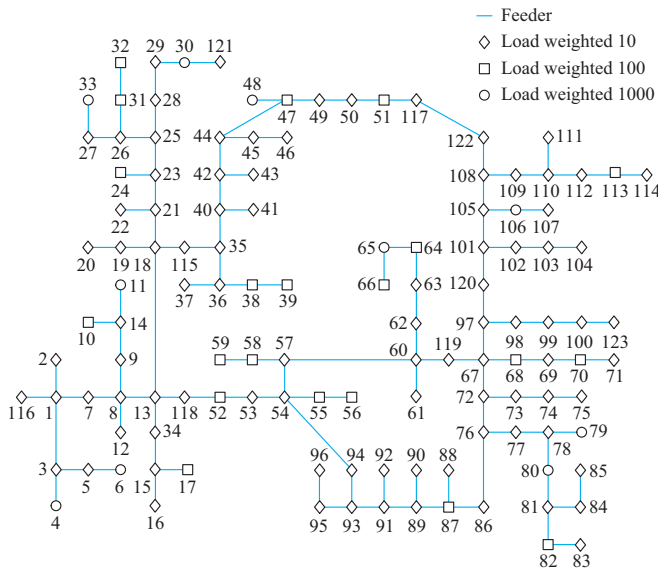


Fig. 6. Topology of modified IEEE 123-bus EDS in the normal state.

A. Restoration Scheduling Results with $T_r = 30$ min

With the restoration rolling optimization horizon of $T = 120$ min, the rescheduling time gap T_r is set to 30 min, and the restoration scheduling is started at $t_c = 0$ min and updated at $t_c = 30$ min, 60 min, 90 min, etc. The restoration scheduling of the test system is completed through the multi-agent-based rolling optimization process proposed in Section III. The detailed restoration results at four sequential restora-

tion scheduling (start) and rescheduling moments, i.e., $t_c = 0$ min, 30 min, 60 min, and 90 min, are summarized and analyzed.

In the figures depicting the system, different shapes of the buses represent different priorities. A dotted blue line between two bus agents means that there is a communication link between the two agents and the feeder between the two buses is available. A solid green line means that the feeder is energized. All the DGs are represented as red circles, while the red star represents ES. The shade of the bus symbol corresponds to the percentage of the load restored at the bus. The darker the shade, the higher the percentage of the load restored at the bus. For the bus with an ES, the shade of the star symbol illustrates the percentage of energy remained. In the figures depicting the performance of the consensus algorithm, changes in the inverse number of the indicator of each agent are illustrated.

1) Restoration Results at $t_c = 0$ min

The restoration of the test system is supposed to be started at $t_c = 0$ min. Figures 7 and 8 show IDP results of the test system at $t_c = 0$ min. According to Fig. 7, there are 3 CCPs in EDS, and each has 13, 10 and 6 agents, respectively. Figure 8 shows the agents and connections available at $t_c = 0$ min. In total, 3 DGs and 1 ES are discovered and available for load restoration in EDS. The major parameters of DGs and ES are listed in Tables II and III. $t_{DG,start}^{t_c}$ of the DG on Bus 8 is negative, which means that it starts 10 min before it is discovered at $t_c = 0$ min by IDP. And the actual restoration results of the test system at $t_c = 0$ min are summarized in Table IV.

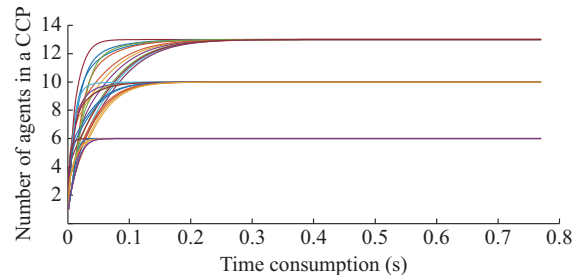


Fig. 7. Performance of average consensus algorithm in identifying CCPs at the first scheduling moment $t_c = 0$ min in $T = [0, 120]$ min.

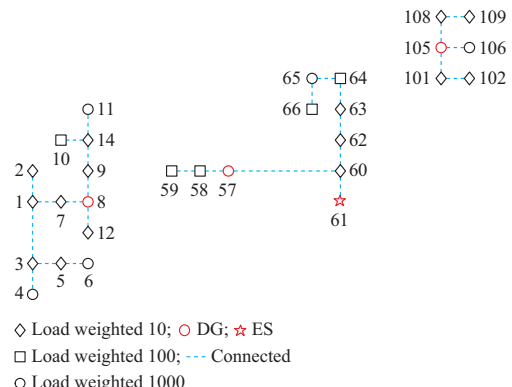


Fig. 8. Identified and restoration results of CCPs at $t_c = 0$ min.

TABLE II
PARAMETERS OF DISCOVERED ES AT BUS 61 IN TEST EDS AT $t_c = 0$ MIN

C_{ES} (kWh)	$P_{ES, ch}^{\max}$ (kW)	$P_{ES, dis}^{\max}$ (kW)	Q_{\max} (kvar)	η_{ch}	η_{dis}	$SOC_{ES, \max}$	$SOC_{ES, \min}$	SOC_{ES}^0
200	50	50	50	0.85	1.15	0.95	0.05	0.80

TABLE III
PARAMETERS OF DISCOVERED DGs IN TEST EDS AT $t_c = 0$ MIN

Bus	P_{\max} (kW)	P_{\min} (kW)	Q_{\max} (kvar)	$P_{DC, damp}^{\max}$ (kW/min)	T_{DG}^{syn} (min)	$t_{DG, \text{start}}^{t_c}$ (min)
8	200	33.3	150	11.1	10	-10
57	300	66.7	200	16.7	15	0
105	200	33.3	150	11.1	10	0

TABLE IV
ACTIVE POWER OUTPUTS OF DGs AND ES AND DIFFERENT CLASS LOAD RESTORATION RESULTS AT $t_c = 0$ MIN

t_c (min)	$\sum_{i \in S_{\text{bus}}^c} P_{G,i}^{t_c}$ (kW)	$\sum_{i \in S_{\text{bus}}^c} P_{L1,i}^{t_c}$ (kW)	$\sum_{i \in S_{\text{bus}}^c} P_{L2,i}^{t_c}$ (kW)	$\sum_{i \in S_{\text{bus}}^c} P_{L3,i}^{t_c}$ (kW)
0	0	0	0	0

2) Restoration Results at $t_c = 30$ min

As T_r is set to 30 min, the restoration schedules should be updated at $t_c = 30$ min. Table V summarizes the actual restoration results of the test system at $t_c = 30$ min according to the optimized EDS restoration schedules determined at $t_c = 0$ min. Based on the restoration results, referring to Fig. 5, IDP is implemented to update the system state information at $t_c = 30$ min.

TABLE V
ACTIVE POWER OUTPUTS OF DGs AND ES AND DIFFERENT CLASS LOAD RESTORATION RESULTS AT $t_c = 30$ MIN

t_c (min)	$\sum_{i \in S_{\text{bus}}^c} P_{G,i}^{t_c}$ (kW)	$\sum_{i \in S_{\text{bus}}^c} P_{L1,i}^{t_c}$ (kW)	$\sum_{i \in S_{\text{bus}}^c} P_{L2,i}^{t_c}$ (kW)	$\sum_{i \in S_{\text{bus}}^c} P_{L3,i}^{t_c}$ (kW)
30	600.1	300	170.9	124.6

Figures 9 and 10 show the IDP results of the test system at $t_c = 30$ min. The DG with the parameters in Table VI is newly discovered and available for load restoration in the later restoration intervals. Based on the new information, the restoration schedule for EDS in the following $T = [30, 150]$ min is updated at $t_c = 30$ min.

3) Restoration Results at $t_c = 60$ min

Table VII summarizes the actual restoration results of the test system at $t_c = 60$ min. Based on the restoration results, IDP is implemented to update the system state information at $t_c = 60$ min. Figures 11 and 12 show the IDP results of the test system at $t_c = 60$ min. DGs with the parameters in Table VIII are newly discovered and available for load restoration in the later restoration intervals.

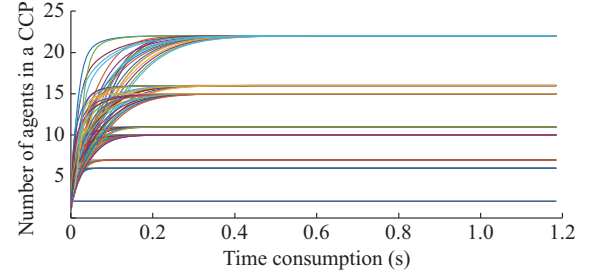


Fig. 9. Performance of average consensus algorithm in identifying CCPs at the first scheduling moment $t_c = 30$ min in $T = [30, 150]$ min.

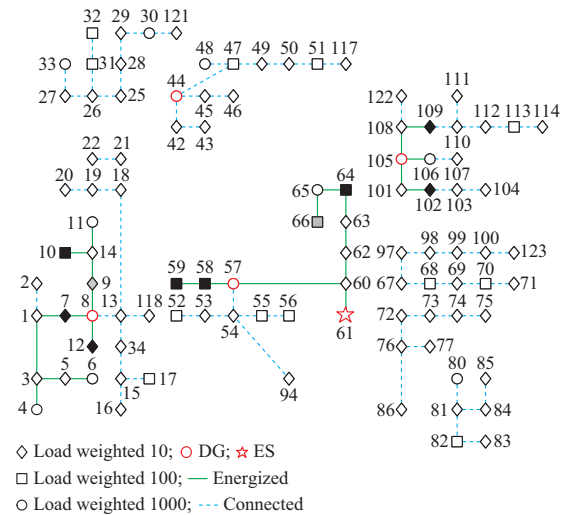


Fig. 10. CCPs identified and restoration results at $t_c = 30$ min.

TABLE VI
PARAMETERS OF NEWLY DISCOVERED DG IN TEST EDS AT $t_c = 30$ MIN

Bus	P_{\max} (kW)	P_{\min} (kW)	Q_{\max} (kvar)	$P_{DG, \text{ramp}}^{\max}$ (kW/min)	T_{DG}^{syn} (min)	$t_{DG, \text{start}}^{t_c}$ (min)
44	150	16.7	100	8.3	10	15

TABLE VII
ACTIVE POWER OUTPUTS OF DGs AND ES AND DIFFERENT CLASS LOAD RESTORATION RESULTS AT $t_c = 60$ MIN

t_c (min)	$\sum_{i \in S_{\text{bus}}^c} P_{G,i}^{t_c}$ (kW)	$\sum_{i \in S_{\text{bus}}^c} P_{L1,i}^{t_c}$ (kW)	$\sum_{i \in S_{\text{bus}}^c} P_{L2,i}^{t_c}$ (kW)	$\sum_{i \in S_{\text{bus}}^c} P_{L3,i}^{t_c}$ (kW)
60	900	410.6	285.8	198.2

4) Restoration Results at $t_c = 90$ min

Table IX summarizes the actual restoration results of the test system at $t_c = 90$ min. On the basis of the restoration results, IDP is implemented to update the system state information at $t_c = 90$ min, and the corresponding results are shown in Fig. 13 and 14. Referring to Fig. 4, the restoration schedules will be successively updated at $t_c = 120$ min, 150 min, 180 min, etc., unless the rolling optimization terminal condition is met, e.g., the power supply from the transmission network is recovered.

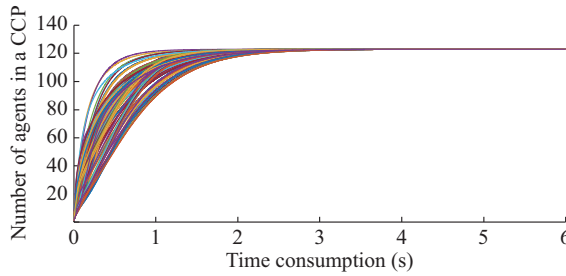


Fig. 11. Performance of average consensus algorithm in identifying CCPs at the first scheduling moment $t_c = 60$ min in $T = [60, 180]$ min.

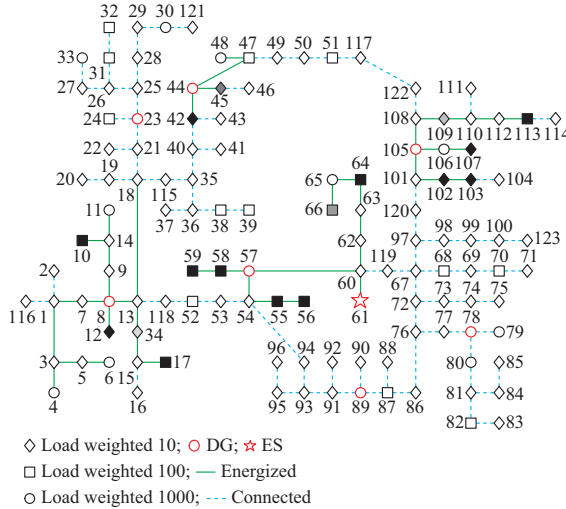


Fig. 12. CCPs identified and restoration results at $t_c = 60$ min.

TABLE VIII

PARAMETERS OF NEWLY DISCOVERED DG IN TEST EDS AT $t_c = 60$ MIN

Bus	P_{\max} (kW)	P_{\min} (kW)	Q_{\max} (kvar)	$P_{\text{DG,ramp}}^{\max}$ (kW/min)	$T_{\text{DG}}^{\text{syn}}$ (min)	$t_{\text{DG,start}}^{t_c}$ (min)
23	100	5.6	60	5.6	5	40
78	120	13.3	100	6.7	10	50
89	120	13.3	100	6.7	10	20

TABLE IX

ACTIVE POWER OUTPUTS OF DGs AND ES AND DIFFERENT CLASS LOAD RESTORATION RESULTS AT $t_c = 90$ MIN

t_c (min)	$\sum_{i \in S_{\text{bus}}^c} P_{G,i}^{t_c}$ (kW)	$\sum_{i \in S_{\text{bus}}^c} P_{L1,i}^{t_c}$ (kW)	$\sum_{i \in S_{\text{bus}}^c} P_{L2,i}^{t_c}$ (kW)	$\sum_{i \in S_{\text{bus}}^c} P_{L3,i}^{t_c}$ (kW)
90	1227.1	670.0	503.8	47.3

It is important to note that in the performance of the average consensus algorithm for identifying CCPs at different t_c in Figs. 7, 9, 11, and 13, considering that the wireless communication latency is less than 1 ms when supported by next-generation communication technology [27], the time span of each iteration in (53) is set as 1 ms. In accordance with Figs. 7, 9, 11, and 13, the detailed iteration numbers and time costs of the consensus processes at different t_c are

listed in Table X. The time cost of the consensus processes makes up the majority of the IDP time span. Compared to Δt and T_r in the rolling optimization method, the time span for IDP can be neglected, which ensures the effectiveness of the proposed multi-agent-based rolling optimization method in EDS restoration scheduling.

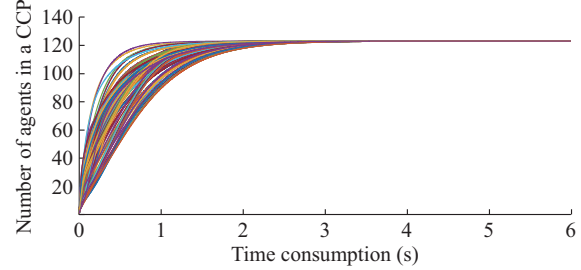


Fig. 13. Performance of average consensus algorithm for identifying CCPs at the first scheduling moment $t_c = 90$ min in $T = [90, 210]$ min.

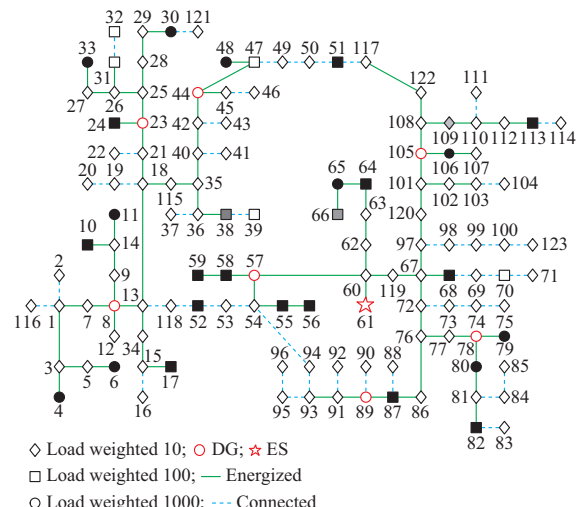


Fig. 14. CCPs identified and restoration results at $t_c = 90$ min.

TABLE X
DETAILED INFORMATION ABOUT CONSENSUS PROCESS AT DIFFERENT t_c

t_c (min)	Iteration number	Time (s)
0	770	0.8
30	1184	1.2
60	6290	6.3
90	6290	6.3

B. Restoration Scheduling Results under $T_r = 45$ min

To further analyze the features of the proposed rolling optimization restoration scheduling method, the rescheduling time gap is set to be 45 min in this paper for comparison. The restoration results at $t_c = 0$ min with $T_r = 45$ min are the same as those with $T_r = 30$ min in the first subsection of Section IV-A. Similar to the rolling process in Section IV-A, the restoration results for the test system at $t_c = 45$ min and 90 min with $T_r = 45$ min are briefly shown in Figs. 15 and 16 and Tables XI-XIV.

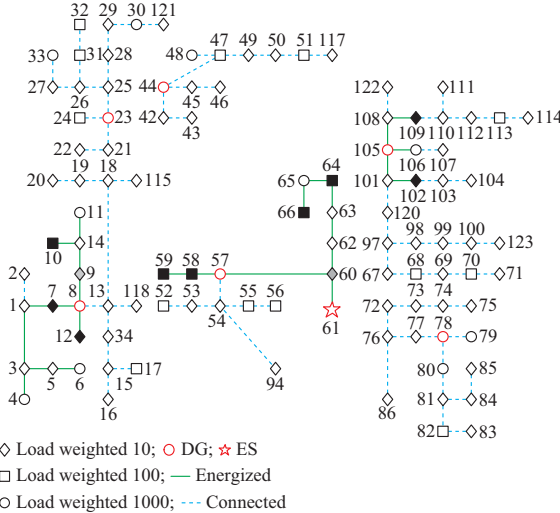


Fig. 15. CCPs identified and restoration results at $t_c = 45$ min under $T_r = 45$ min.

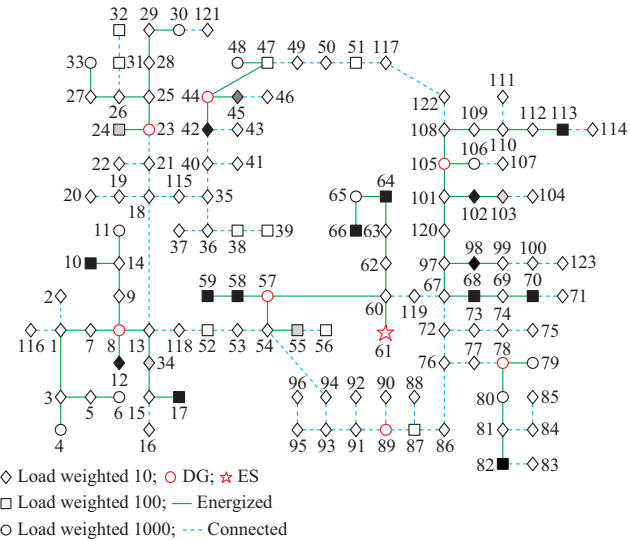


Fig. 16. CCPs identified and restoration results at $t_c = 90$ min under $T_r = 45$ min.

TABLE XI

ACTIVE POWER OUTPUTS OF DGs AND ES AND DIFFERENT CLASS LOAD RESTORATION RESULTS AT $t_c = 45$ MIN UNDER $T_r = 45$ MIN

t_c (min)	$\sum_{i \in S_{\text{bus}}^{t_c}} P_{G,i}^{t_c}$ (kW)	$\sum_{i \in S_{\text{bus}}^{t_c}} P_{L1,i}^{t_c}$ (kW)	$\sum_{i \in S_{\text{bus}}^{t_c}} P_{L2,i}^{t_c}$ (kW)	$\sum_{i \in S_{\text{bus}}^{t_c}} P_{L3,i}^{t_c}$ (kW)
45	650.1	300	210	134

The comparison of the load restoration results of the test system at $t_c = 90$ min with different set values of T_r (30 min and 45 min) is shown in Table XV. At $t_c = 90$ min, the sum of the first-class loads restored (third column in Table XV), the sum of the second-class loads restored (fourth column), and the total loads restored (sixth column) in the load restoration results with $T_r = 30$ min are larger than those in the $T_r = 45$ min case, demonstrating a better restoration perfor-

mance.

TABLE XII
PARAMETERS OF NEWLY DISCOVERED DGs IN TEST EDS
AT $t_c = 45$ MIN UNDER $T_r = 45$ MIN

Bus	P_{\max} (kW)	P_{\min} (kW)	Q_{\max} (kvar)	$P_{\text{DG,ramp}}^{\max}$ (kW/min)	$T_{\text{DG}}^{\text{syn}}$ (min)	$t_{\text{DG,start}}^{t_c}$ (min)
23	100	5.6	60	5.6	5	40
44	150	16.7	100	8.3	10	15
78	120	13.3	100	6.7	10	50

TABLE XIII
ACTIVE POWER OUTPUTS OF DGs AND ES AND DIFFERENT CLASS LOAD RESTORATION RESULTS AT $t_c = 90$ MIN UNDER $T_r = 45$ MIN

t_c (min)	$\sum_{i \in S_{\text{bus}}^{t_c}} P_{G,i}^{t_c}$ (kW)	$\sum_{i \in S_{\text{bus}}^{t_c}} P_{L1,i}^{t_c}$ (kW)	$\sum_{i \in S_{\text{bus}}^{t_c}} P_{L2,i}^{t_c}$ (kW)	$\sum_{i \in S_{\text{bus}}^{t_c}} P_{L3,i}^{t_c}$ (kW)
90	1118	570.6	378.5	162.2

TABLE XIV
PARAMETERS OF NEWLY DISCOVERED DGs IN TEST EDS
AT $t_c = 90$ MIN UNDER $T_r = 45$ MIN

Bus	P_{\max} (kW)	P_{\min} (kW)	Q_{\max} (kvar)	$P_{\text{DG,ramp}}^{\max}$ (kW/min)	$T_{\text{DG}}^{\text{syn}}$ (min)	$t_{\text{DG,start}}^{t_c}$ (min)
89	120	13.3	100	6.7	10	20

TABLE XV
LOAD RESTORATION RESULTS OF TEST SYSTEM AT $t_c = 90$ MIN
UNDER $T_r = 30$ MIN AND $T_r = 45$ MIN

t_c (min)	T_r (min)	$\sum_{i \in S_{\text{bus}}^{t_c}} P_{L1,i}^{t_c}$ (kW)	$\sum_{i \in S_{\text{bus}}^{t_c}} P_{L2,i}^{t_c}$ (kW)	$\sum_{i \in S_{\text{bus}}^{t_c}} P_{L3,i}^{t_c}$ (kW)	$\sum_{i \in S_{\text{bus}}^{t_c}} P_{L4,i}^{t_c}$ (kW)
90	30	670.0	503.8	47.3	1221.1
90	45	570.6	378.5	162.2	1111.3

Referring to Tables II, III, VI, and VIII in Section IV-A and Tables XII and XIV in this part, the rolling optimization restoration processes can consider the new restoration resources (e.g., newly discovered DGs/ESs, reenergized or repaired agents, repaired buses/feeders) during the whole restoration, which effectively enhances the restoration performance.

In general, a shorter T_r leads to a better restoration performance. An adequate frequency of rescheduling should be considered in practical EDS restoration. Considering the set values of Δt ($\Delta t = 5$ min or 10 min in practical restoration), frequent rescheduling ($T_r \leq 15$ min) is unnecessary and will increase the pressure on the communication system. For the set value of $\Delta t = 5$ min in the case study, the set value of $T_r = 30$ min can yield a satisfying restoration performance of the test system.

V. CONCLUSION

A multi-agent-based rolling optimization method for restoration scheduling of an EDS with distributed generation is

proposed in this paper. Considering the risk of losing the centralized authority due to the failure of the core communication network, an MAS with distributed communication is introduced, and a rolling optimization process is newly established to achieve decentralized decision-making for EDS restoration scheduling. Through decentralized decision-making and rolling optimization, EDS restoration scheduling can be automatically started and can periodically update itself, providing an effective solution for EDS restoration scheduling in a blackout event.

The proposed method is verified on a modified IEEE 123-bus EDS. In the case studies, the steps of the multi-agent-based rolling optimization method for EDS restoration scheduling are illustrated by detailed restoration results at four sequential restoration scheduling/rescheduling moments in the rolling process. Case studies demonstrate that the rolling restoration optimization process can consider new restoration resources to participate in the restoration in a timely manner and effectively enhance the restoration performance. To analyze the influence of the communication latency on the rolling restoration optimization process, the convergence and time cost of the average consensus algorithm for IDP during restoration scheduling are studied. Comparisons between restoration scheduling results for the test system under different rescheduling time gaps are also included in the case studies to demonstrate the features of the proposed EDS restoration scheduling method.

From the perspective of resilience, the multi-agent-based restoration scheduling method can overcome the unreliability of centralized restoration scheduling after disasters. The rolling optimization process can consider new restoration resources in EDS through periodically updating the restoration schedule. This paper mainly focuses on the load restoration of EDS in the earlier restoration stages after a blackout. Future works will include the coordination of EDS restoration with transmission system restoration. The uncertainty of the distributed generation in EDS restoration will also be studied.

REFERENCES

- [1] L. Che, M. Khodayar, and M. Shahidehpour, "Only connect: microgrids for distribution system restoration," *IEEE Power and Energy Magazine*, vol. 12, no. 1, pp. 70-81, Feb. 2014.
- [2] Energy Technology Laboratory. (2009, Sept.). Operates resiliently against attack and natural disaster. [Online]. Available: http://www.smartgridinformation.info/pdf/1438_doc_1.pdf
- [3] M. F. Ahern, "Cybersecurity in power systems," *IEEE Potentials*, vol. 36, no. 5, pp. 8-12, Oct. 2017.
- [4] R. Yan, N. A. Masood, T. K. Saha *et al.*, "The anatomy of the 2016 South Australia blackout: a catastrophic event in a high renewable network," *IEEE Transactions on Power Systems*, vol. 33, no. 5, pp. 5374-5388, Sept. 2018.
- [5] X. Cheng, K. Ning, W. Duan *et al.*, "Design and realization for fault restoration system based on the genetic algorithm," in *Proceedings of IEEE International Conference on Information and Automation*, Ningbo, China, Aug. 2016, pp. 905-909.
- [6] I. Sadeghkhani, A. Ketabi, and R. Feuillet, "The study of switching overvoltages under power system restoration scenario using extended delta-bar-delta algorithm," *International Journal of Emerging Electric Power Systems*, vol. 14, no. 3, pp. 219-230, Jul. 2013.
- [7] G. H. Reddy, P. Chakrapani, A. K. Goswami *et al.*, "Fuzzy based approach for restoration of distribution system during post natural disasters," *IEEE Access*, vol. 6, pp. 3448-3458, Dec. 2017.
- [8] M. Z. A. El-Hamed, W. El-Khattam, and R. El-Sharkawy, "Self-healing restoration of a distribution system using hybrid fuzzy control/ant colony optimization algorithm," in *Proceedings of 2013 3rd International Conference on Electric Power and Energy Conversion Systems*, Istanbul, Turkey, Oct. 2013, pp. 1-6.
- [9] D. Sijivac, S. Nikolovski, and Z. Kovac, "Distribution network restoration using sequential Monte Carlo approach," in *Proceedings of 2006 International Conference on Probabilistic Methods Applied to Power Systems*, Stockholm, Sweden, Jun. 2006, pp. 1-6.
- [10] S. B. Elghali, R. Ooubib, and M. Benbouzid, "Selecting and optimal sizing of hybridized energy storage systems for tidal energy integration into power grid," *Journal of Modern Power Systems and Clean Energy*, vol. 7, no. 1, pp. 113-122, Jan. 2019.
- [11] K. Chen, W. Wu, B. Zhang *et al.*, "Robust restoration decision-making model for distribution networks based on information gap decision theory," *IEEE Transactions on Smart Grid*, vol. 6, no. 2, pp. 587-697, Mar. 2015.
- [12] H. Gao, Y. Chen, Y. Xu *et al.*, "Resilience-oriented critical load restoration using microgrids in distribution systems," *IEEE Transactions on Smart Grid*, vol. 7, no. 6, pp. 2837-2848, Nov. 2016.
- [13] H. Farzin, M. Fotuhi-Firuzabad, and M. Moeini-Aghtaie, "Enhancing power system resilience through hierarchical outage management in multi-microgrids," *IEEE Transactions on Smart Grid*, vol. 7, no. 6, pp. 2869-2879, Nov. 2016.
- [14] C. Chen, J. Wang, F. Qiu *et al.*, "Resilient distribution system by microgrids formation after natural disasters," *IEEE Transactions on Smart Grid*, vol. 7, no. 2, pp. 958-966, Mar. 2016.
- [15] Y. Xu and W. Liu, "Novel multiagent based load restoration algorithm for microgrid," *IEEE Transactions on Smart Grid*, vol. 2, no. 1, pp. 152-161, Mar. 2011.
- [16] J. Silvente, G. M. Kopanos, E. N. Pistikopoulos *et al.*, "A rolling horizon optimization framework for the simultaneous energy supply and demand planning in microgrids," *Applied Energy*, vol. 155, pp. 485-501, Oct. 2015.
- [17] P. Chen, Y.-Q. Bao, X. Zhu *et al.*, "Day-ahead scheduling of large numbers of thermostatically controlled loads based on equivalent energy storage model," *Journal of Modern Power Systems and Clean Energy*, vol. 7, no. 3, pp. 579-588, May 2019.
- [18] Y. Zhou, J. Yun, Z. Yan *et al.* (2018, Sept.). Self-optimal piecewise linearization based network power flow constraints in electrical distribution system optimization. [Online]. Available: <http://cn.arxiv.org/ftp/arxiv/papers/1809/1809.02367.pdf>
- [19] C. Chen, J. Wang, and D. Ton, "Modernizing distribution system restoration to achieve grid resiliency against extreme weather events: an integrated solution," *Proceedings of the IEEE*, vol. 105, no. 7, pp. 1267-1288, Jul. 2017.
- [20] M. Lavorato, J. F. Franco, M. J. Rider *et al.*, "Imposing radiality constraints in distribution system optimization problems," *IEEE Transactions on Smart Grid*, vol. 27, no. 1, pp. 172-180, Feb. 2012.
- [21] Z. Hu, R. Guo, H. Lan *et al.*, "Islanding model of distribution systems with distributed generators based on directed graph," *Automation of Electric Power Systems*, vol. 39, no. 14, pp. 97-104, Jul. 2015.
- [22] J. S. Kim and T. F. Edgar, "Optimal scheduling of combined heat and power plants using mixed-integer nonlinear programming," *Energy*, vol. 77, pp. 675-690, Oct. 2014.
- [23] M. Bahrman and P. E. Bjorklund, "The new black start: system restoration with help from voltage-sourced converters," *IEEE Power and Energy Magazine*, vol. 12, no. 1, pp. 44-53, Feb. 2014.
- [24] H. Jiang, Y. Gao, G. Zhang *et al.*, "A zone-based intrusion detection system for wireless ad hoc distribution power communication networks," in *Proceedings of 2005 IEEE PES Transmission and Distribution Conference; Exposition: Asia and Pacific*, Dalian, China, Aug. 2005, pp. 1-6.
- [25] L. Xiao, S. Boyd, S. J. Kim *et al.*, "Distributed average consensus with least-mean-square deviation," *Journal of Parallel and Distributed Computing*, vol. 67, no. 1, pp. 33-46, 2007.
- [26] X. Xiao, "Research on coordinated planning of power system with wind farms and vehicles," M.S. thesis, Department of Electrical Engineering, Zhejiang University, Zhejiang, China, 2014.
- [27] M. Agiwal, A. Roy, and N. Saxena, "Next generation 5G wireless networks: a comprehensive survey," *IEEE Communications Surveys and Tutorials*, vol. 18, no. 3, pp. 1617-1655, Aug. 2016.

Donghan Feng received the B.S. and Ph.D. degrees from the Department of Electrical Engineering, Zhejiang University, Hangzhou, China, in 2003 and 2008, respectively. He has been with the faculty of Shanghai Jiao Tong University, Shanghai, China, since 2008, where he currently is a full profes-

sor. He also serves as the Deputy Director of the State Energy Smart Grid Research and Development Center, Shanghai, China. He was a Graduate Research Assistant with Tsinghua University, Beijing, China, from 2005 to 2006, a Visiting Scholar with the University of Hong Kong, Hong Kong, China, from 2006 to 2007, a Hans Christened Ørsted Postdoc with Technical University of Denmark, Lyngby, Denmark, from 2009 to 2010, a Visiting Research Scholar with the University of California, Berkely, USA, from 2015 to 2016. His research interests include spot pricing in smart energy networks.

Fan Wu received the B.S. degree in electrical engineering from Shanghai Jiao Tong University, Shanghai, China, in 2017. Currently, he is pursuing the M.S. degree with the Key Laboratory of Control of Power Transmission and Conversion, Ministry of Education, Department of Electrical Engineering, Shanghai Jiao Tong University. His research interests include the power system optimization, hybrid renewable energy system and energy storage systems.

Yun Zhou received the B.S. (Hons.) and Ph.D. degrees in electrical engineering from Shanghai Jiao Tong University, Shanghai, China, in 2012 and 2017, respectively. He participated in the joint Ph.D. program of Alstom Grid Technology Center Co., Ltd. and Shanghai Jiao Tong University from Sep. 2013 to Jun. 2017. He was an R&D intern of Alstom Grid China Technology Center from Sep. 2013 to Oct. 2015, and was an R&D intern of GE Grid Solutions China Technology Center from Nov. 2015 to Jun. 2017. He has joined the faculty of the Electrical Engineering Department, Shanghai Jiao Tong University as a Lecturer since Dec. 2017. His current research inter-

ests include power system restoration and energy internet.

Usama Rahman received the B.S. degree in electrical power engineering from the National University of Science Technology, Karachi, Pakistan, in 2013, and the M.S. degree in electrical power systems from the North China Electric Power University, Beijing, China, in 2017. He is currently pursuing the Ph.D. degree in power system engineering from, Shanghai Jiao Tong University, Shanghai, China. He is also a part of faculty development programme from National University of Sciences and Technology, Pakistan. His research interests include electrical power optimization, energy storage systems, artificial intelligence, hybrid renewable energy system and energy storage systems.

Xiaojin Zhao received the B.S. degree in electrical engineering from Shanghai Jiao Tong University, Shanghai, China, in 2019. Currently, she is pursuing the M.S. degree with the Key Laboratory of Control of Power Transmission and Conversion, Ministry of Education, Department of Electrical Engineering, Shanghai Jiao Tong University. Her current research interests include the modeling and optimization of the energy internet.

Chen Fang received the B.S. and Ph.D. degrees from the Department of Electrical Engineering, Tsinghua University, Beijing, China, in 2006 and 2011, respectively. He is currently an Electrical Engineer with the Electric Power Research Institute, State Grid Shanghai Municipal Electric Power Company, Shanghai, China. His current research interests include renewable energy integration of smart grid and power storage technology.